

An extremum method for bending-wrinkling predictions of inflated conical cantilever beam

Changuo Wang^{*1,2}, Zhenyong Du¹ and Huifeng Tan^{2a}

¹Center for Composite Materials, Harbin Institute of Technology, Harbin, 150080 China

²National Key Laboratory of Science and Technology on Advanced Composites in Special Environments, Harbin Institute of Technology, Harbin, 150080 China

(Received January 20, 2011, Revised January 12, 2013, Accepted March 6, 2013)

Abstract. An extremum method is presented to predict the wrinkling characteristics of the inflated cone in bending. The wrinkling factor is firstly defined so as to obtain the wrinkling condition. The initial wrinkling location is then determined by searching the maximum of the wrinkling factor. The critical wrinkling load is finally obtained by determining the ratio of the wrinkling moment versus the initial wrinkling location. The extremum method is proposed based on the assumption of membrane material of beam wall, and it is extended to consider beam wall with thin-shell material in the end. The nondimensional analyses show that the initial wrinkling location is closely related to the taper ratio. When the taper ratio is higher than the critical value, the initial wrinkles will be initiated at a different location. The nondimensional critical wrinkling load nonlinearly increases as the taper ratio increases firstly, and then linearly increases after the critical taper ratio. The critical taper ratio reflects the highest load-carrying efficiency of the inflated cone in bending, and it can be regarded as a measure to optimize the geometry of the inflated cone. The comparative analysis shows fairly good agreement between analytical and numerical results. Over the whole range of the comparison, the mean differences are lower than 3%. This gives confidence to use extremum method for bending-wrinkling analysis of inflated conical cantilever beam.

Keywords: inflated conical cantilever beam; wrinkling; membrane; thin-shell; load-carrying efficiency

1. Introduction

The inflated booms are used to support tents used for temporary medical facilities, disaster-relief shelters, and military applications (Hampel *et al.* 1996, Quigley *et al.* 2003). In recent years, the inflated booms have received widely attentions in applications of inflatable space-based structures including inflatable antennas, solar sails, truss structures and inflatable wings (Jenkins 2001, 2006, Norris and Pulliam 2009) etc. As a supported component, the inflated booms need to meet high load-carrying efficiency and wrinkle-free requirements. However, the inflated booms are typical thin-walled structures which are very easy to be wrinkled. The inflated booms subject to bending were found to develop short wavelength periodic ripples on the compressed side, and the inflated booms buckled locally and collapsed soon after the appearance of the wrinkles (Wang

*Corresponding author, Associate Professor, E-mail: wangcg@hit.edu.cn

^aProfessor, E-mail: tanhf@hit.edu.cn

et al. 2006, 2007, 2009b). Accurate evaluation of bending-wrinkling characteristics is important for better understanding the load-carrying ability of inflated booms.

For inflated beams, bending-wrinkling behavior may be divided into problems in which the wall material is regarded as either a true membrane or a thin-shell, which result in two cases, that is, the membrane case (Stein and Hedgepeth 1961, Comer and Levy 1963, Main *et al.* 1994, Wang *et al.* 2008, 2009c) and the thin-shell case (Wang *et al.* 2009a, Wood 1958, Zender 1962, Wielgosz and Thomas 2002, 2004, Veldman *et al.* 2005, 2006a, b). The distinctions between these two cases are depending on whether the bending and compression stiffness of the beam wall material are considered or not. The wrinkling predictions using these two cases are both based on beam stress analysis. During beam stress analysis, three different stress states can be observed when the beam is bent: the taut state, the partially wrinkled state and the collapsed state. Based on the membrane assumption, the wrinkles will immediately occur when the beam wall material is compressed (Stein and Hedgepeth 1961, Main *et al.* 1994, Wang *et al.* 2008). Based on the thin-shell assumption, the wrinkles will occur when the compressive stress reaches a critical value, which is the local buckling stress. (Wang *et al.* 2009a, Thomas and Wielgosz 2004, Veldman *et al.* 2006a). The axial stress of inflated beam may be obtained by adding the stress of a pressurized membrane to the stress of an unpressurized thin-shell (Wood 1958, Zender 1962). The stress analysis based on the membrane assumption corresponds to the perfect model which is different from the experimental observations. The experimental results reveal that the collapse moment for the pressurized membranes is higher and should be reduced to some a smaller value by multiplying by a modified factor (Thomas and Wielgosz 2004, Veldman *et al.* 2005). Based on the thin-shell assumption, several different formations of the critical compressive stress (Veldman *et al.* 2005, 2006a, b) may be chosen to perform the beam stress analysis. The inflated cone is regarded as the optimum geometry of the straight cylindrical boom, and has the larger possible load-carrying efficiency (Veldman 2003). Several researches on the inflated cones are mainly focused on the predictions on the wrinkling and collapsed moments. These predictions were also compared with the bending experimental results of inflated cones (Veldman *et al.* 2006a, b). However, little work has been done in study of the bending-wrinkling behaviors of the inflated cones.

Increasing use of inflated cones in aerospace application has spurred a need in deeply and accurately evaluating structural properties of inflated conical beams in bending. The purpose of this paper is to presents an approximate formula based on beam stress analysis for accurately predicting bending-wrinkling characteristics of inflated beam. The nonlinear shell finite element numerical computations on the inflated cone are used to verify the accuracy of our approximate formula. The understanding of bending-wrinkling behaviors will be helpful to design a wrinkle-free inflated beam.

2. Beam stress analysis

The inflated cone under bending is shown in Fig. 1. As shown in Fig. 1, r_0 and r_1 are the free-end and the fixed-end radius of an inflated cone, respectively. α is the half cone angle. r is the cross-sectional radius at point A. t is the wall thickness of the inflated cone. P is the inflated pressure.

When the tip transverse load F isn't taken account, the force equilibrium of the inflated cone is given by

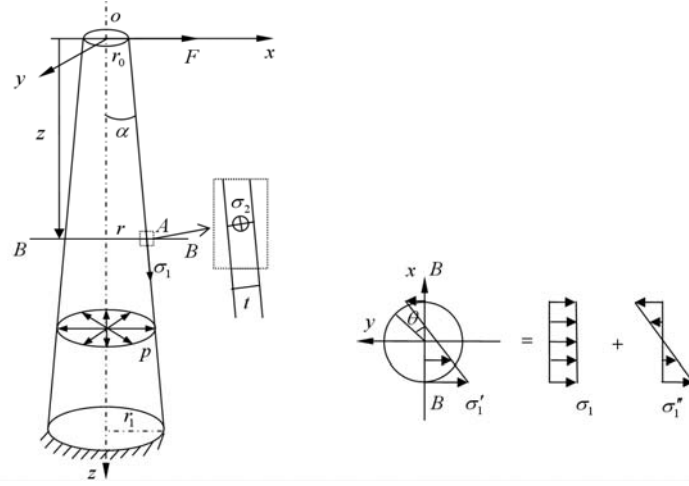


Fig. 1 Inflated conical cantilever beam under bending

$$\frac{\sigma_1}{R_1} + \frac{\sigma_2}{R_2} = \frac{p}{t} \tag{1}$$

Where, the subscripts 1 and 2 denote the axial and hoop coordinates, respectively. The axial stress σ_1 is obtained as follows

$$\sigma_1 = \frac{2\pi \int_0^r pr dr}{2\pi r t \cos \alpha} = \frac{\int_0^r pr dr}{r t \cos \alpha} \tag{2}$$

At point A, the first and the second radius of curvature are expressed as

$$R_1 = \infty, \quad R_2 = r / \cos \alpha \tag{3}$$

The stress at point A can be obtained by substituting Eq. (3) and Eq. (2) into Eq. (1).

$$\sigma_1 = \frac{pr}{2t \cos \alpha}, \quad \sigma_2 = \frac{pr}{t \cos \alpha} \tag{4}$$

In Fig. 1, r_0 is assumed to be constant. Thus, the radius of the inflated cone r can be expressed as a function of the free-end radius r_0 and the axial coordinate z .

$$r = z \tan \alpha + r_0 \quad (0 \leq z \leq z_0) \tag{5}$$

Here, z_0 is the total height of the inflated cone.

$$z_0 = (r_1 - r_0) \cot \alpha \tag{6}$$

At point A (the axial coordinate), the moment M of the inflated cone under tip transverse load F is obtained as

$$M = Fz \tag{7}$$

The moment equilibrium at point A (the axial coordinate z) is then written as

$$M - r^2 t \int_0^{2\pi} \sigma'_1 \cos \alpha \cos \theta d\theta = 0 \quad (8)$$

Where, σ'_1 is the axial stress resultant of the inflated cone.

The wrinkles will be formed when the moment at point A reaches a critical value. The moment corresponding to the first wrinkle is defined as the wrinkling moment, M_w .

A wrinkling factor is defined as the ratio of the moment M at point A versus the wrinkling moment M_w . According to the definition of the wrinkling factor, the wrinkles will occur when $\lambda \geq 1$, which responds to the wrinkling condition.

$$\begin{cases} \lambda \geq 1 & \text{wrinkling} \\ \lambda < 1 & \text{no wrinkling} \end{cases} \quad (9)$$

Based on the wrinkling condition (Eq.(9)), the wrinkles will be firstly formed when the wrinkling factor reaches its maximum. Thus, the initial wrinkling location can be indirectly obtained by searching the extremum (the maximum) of the wrinkling factor, which is named as the extremum method.

The maximum of the wrinkling factor can be obtained and expressed in the form

$$\frac{d\lambda}{dz} = 0 \quad \text{and} \quad \frac{d^2\lambda}{dz^2} < 0 \quad (10)$$

3. Bending-wrinkling characteristics analysis

Based on above beam stress analysis, we use membrane and thin-shell to consider the beam wall material, respectively, which results in two cases. During wrinkling analysis, these two cases correspond to different wrinkling criterions. Further, the distinction between thin-shell and membrane cases is only that in the former wrinkling is defined to occur at a specified maximum compressive stress while in the latter that maximum is taken to be zero (Stein and Hedgepeth 1961, Wang *et al.* 2008).

The wrinkling criterion for isotropic membrane is given by

$$\min(\sigma'_1) = \begin{cases} 0 & \text{membrane case} \\ -\sigma_{cr} & \text{thin shell case} \end{cases} \quad (11)$$

The axial stress resultant of the inflated cone, σ'_1 , may be decomposed into two parts: the stress σ_1 due to inflated pressure P and the stress σ''_1 due to tip transverse load F .

$$\sigma'_1 = \sigma_1 + \sigma''_1 = \frac{Pr}{2t \cos \alpha} + C_0 \cos \theta \quad (12)$$

C_0 can be determined according to the wrinkling stress criterion (Eq. (11)).

$$\sigma'_1 = \begin{cases} \frac{pr}{2t \cos \alpha} (1 - \cos \theta) & \text{membrane case} \\ \frac{pr}{2t \cos \alpha} (1 - \cos \theta) - \sigma_{cr} \cos \theta & \text{thin shell case} \end{cases} \quad (13)$$

Further, the wrinkling moment can be obtained by substituting Eq. (13) into Eq. (8).

$$M_w = \begin{cases} \frac{1}{2} p \pi r^3 & \text{membrane case} \\ \frac{1}{2} p \pi r^3 + \pi r^2 t \sigma_{cr} \cos \alpha & \text{thin shell case} \end{cases} \quad (14)$$

In addition, different from prior definitions of the critical wrinkling load (Veldman *et al.* 2006a, b, Wang *et al.* 2008), the critical wrinkling load F_w in this paper is defined as the ratio of the wrinkling moment M_w versus the initial wrinkling location z_w , which isn't identically equal to the ratio between the wrinkling moment and the total height of the inflated cone.

3.1 Membrane case

For the membrane case, the wrinkling factor can be expressed as

$$\lambda = \frac{M}{M_w} = \frac{2Fz}{p \pi r^3} \quad (15)$$

where, $r = z \tan \alpha + r_0$. Substituting Eq. (15) into Eq. (10), we have

$$\begin{cases} \frac{2F(r_0 - 2z \tan \alpha)}{\pi p (z \tan \alpha + r_0)^4} = 0 \\ -\frac{4F[z(1 - 4 \tan^2 \alpha) + 3r_0 \tan \alpha]}{\pi p (z \tan \alpha + r_0)^5} < 0 \end{cases} \quad (16)$$

Solving the equality of Eq. (16), we get

$$z = \frac{1}{2} r_0 \cot \alpha \quad (17)$$

Substituting Eq. (17) into the inequality of Eq. (16), we find

$$\frac{d^2 \lambda}{dz^2} = -\frac{2F r_0 (\cot \alpha + 2 \tan \alpha)}{\pi p (\frac{3}{2} r_0)^5} \quad (18)$$

Given the case of $r_0 < r_1$, we obtain the condition of $0 < \alpha < \pi/2$. We further determine that the inequality $d^2 \lambda / dz^2 < 0$ is identically satisfied. In other words, the initial wrinkling location is $z_w = r_0 / 2 \cot \alpha$ for the membrane case.

Substituting Eq. (17) into the span of axial coordinate z in Eq. (5) ($0 \leq z \leq z_0$), we have $r_1 \geq 1.5 r_0$

with the condition of $z_w = r_0/2 \cot\alpha$. For the case $r_1 \geq 1.5r_0$, the initial wrinkling location arises at the interior of the inflated cone. For the case $r_0 \leq r_1 \leq 1.5r_0$, the initial wrinkling location z_w obtained from Eq. (17) goes beyond the height limitation of the inflated cone (z_0). For this case, the initial wrinkling location is determined at the fixed-end of the inflated cone, that is $z_w = z_0$. Specially, the initial wrinkling location of an inflated booms ($r_1 = r_0$) in bending is identical at the fixed-end.

The initial wrinkling location can be interpreted by using a concept of the wrinkling hinges. We find that one can make an analogy between plastic hinges and wrinkled regions which arise in inflated beams in bending. When the plasticity appears at the interior of a beam, the load, which gives the beginning of plasticity, seems to the wrinkling load of an inflated beam. When the tip load is increased, the wrinkled region will spreads around the hoop cross-section. This process isn't over until the inflated beam is entirely collapsed. Thus the initial wrinkling location can be regarded as a wrinkling hinge, where the moment is the wrinkling moment.

Next we have the critical wrinkling load

$$F_w = \frac{M_w}{z_w} = \begin{cases} \frac{27}{8} \frac{\pi p r_0^3}{z_0} \left(\frac{r_1}{r_0} - 1 \right) & r_1 \geq 1.5r_0 \\ \frac{\pi p r_0^3}{2z_0} \left(\frac{r_1}{r_0} \right)^3 & r_0 \leq r_1 < 1.5r_0 \end{cases} \quad (19)$$

3.2 Thin-shell case

In using the ‘‘thin-shell model’’, the material is considered as a thin-shell with a small but non-zero bending stiffness. The wrinkles are formed and treated as the local buckling ripples after the minimum principal stress reaches the critical compressive stress σ_{cr} . The thin-shell axial stress resultant and the wrinkling moment may be obtained from Eqs. (13) and (14).

The thin-shell wrinkling condition has the same definition formation as the membrane case. Then we have the thin-shell wrinkling factor

$$\lambda = \frac{M}{M_w} = \frac{2Fz}{p\pi r^3 + 2\pi r^2 t \sigma_{cr} \cos\alpha} \quad (20)$$

Based on the idea of the extremum method, we need obtain the maximum of the wrinkling factor to further determine the initial wrinkling location, z_w . Based upon the extremum condition, Eq.(10), and the thin-shell wrinkling factor, Eq.(20), we have

$$\begin{cases} \frac{2F(A - Bz \tan\alpha)}{A^2} = 0 \\ \frac{-2F(zAC \tan^2\alpha + 2AB \tan\alpha - 2zB^2 \tan^2\alpha)}{A^3} < 0 \end{cases} \quad (21)$$

Here, $A = p\pi r^3 + 2\pi r^2 t \sigma_{cr} \cos\alpha$, $C = B' = A''$.

Under the assumption of infinite inflated pressure, P , solving the equality of Eq. (21), we have

$$z = \left(\frac{r_0}{2} - \frac{\sigma_{cr} t \cos \alpha}{2p} \right) \cot \alpha \quad (22)$$

Substituting Eq. (22) in the in equation of Eq. (21), we find that the in equation of Eq. (21) can also be identically satisfied when $0 < \alpha < \pi/2$. Thus we obtain the thin-shell initial wrinkling

$$\text{location } z_w = \left(\frac{r_0}{2} - \frac{\sigma_{cr} t \cos \alpha}{2p} \right) \cot \alpha .$$

Substituting Eq. (22) in Eq. (5), we also have the thin-shell initial wrinkling location $z_w = \left(\frac{r_0}{2} - \frac{\sigma_{cr} t \cos \alpha}{2p} \right) \cot \alpha$ when $r_1 \geq \frac{3}{2}r_0 - \frac{\sigma_{cr} t \cos \alpha}{2p}$. For this case, the initial wrinkling

location occurs at the interior of the inflated cone. When $r_0 \leq r_1 < \frac{3}{2}r_0 - \frac{\sigma_{cr} t \cos \alpha}{2p}$, we obtain the initial wrinkling location at the fixed-end of the inflated cone, which responds to the case of $z_w = z_0$. For the case of the inflated thin-shell boom, $r_0 = r_1$, the initial wrinkling location is also at its fixed-end identically.

In order to deeply understand the distribution of the initial wrinkling location, we perform a nondimensional analysis of $\bar{z} = z_w/z_0$ versus $\bar{r} = r_1/r_0$. Combining Eq. (6) with Eq. (22), we have

$$\bar{z} = \frac{1 - \xi}{2(\bar{r} - 1)} \quad (23)$$

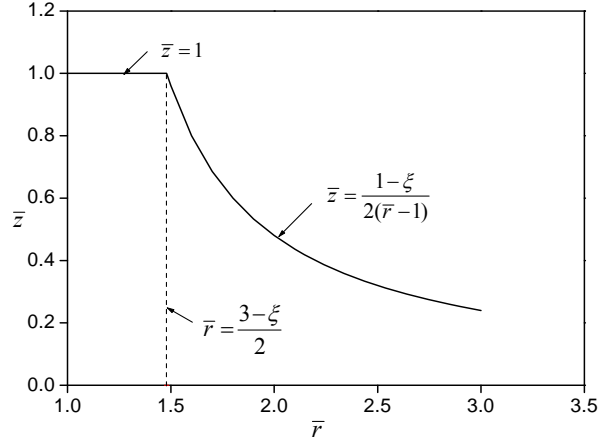
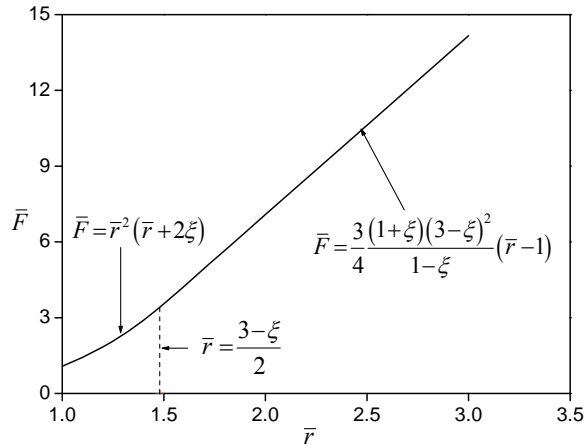
Here, we give $\xi = \frac{\sigma_{cr} t \cos \alpha}{pr_0}$.

We further analyze the nondimensional relationship of \bar{z} versus \bar{r} , and plot it in Fig. 2.

$$\bar{z} = \begin{cases} 1 & (1 \leq \bar{r} < \frac{3 - \xi}{2}) \\ \frac{1 - \xi}{2(\bar{r} - 1)} & (\bar{r} \geq \frac{3 - \xi}{2}) \end{cases} \quad (24)$$

As shown in Fig. 2, the initial wrinkles occur at the fixed-end ($\bar{z} = 1$ or $z_w = z_0$) of the inflated cone when $1 < \bar{r} < 3 - \xi/2$. When $\bar{r} \geq 3 - \xi/2$, the initial wrinkling location is changed from the interior to the free-end of the inflated cone with \bar{r} increases. Thus the taper ratio $\bar{r} = 3 - \xi/2$ is a turning point for the initial wrinkling location. When $\xi = 0$, the thin-shell model is simplified as the membrane model. For the membrane model, $\bar{r} = 1.5$ is the turning point.

For the thin-shell critical wrinkling load, we use the same definition as membrane case in this section. In addition, we use the nondimensional formations of $\bar{F} = 2F_w z_0 / \pi p r_0^3$ versus $\bar{r} = r_1/r_0$ to express the thin-shell critical wrinkling load as follows and plot it in Fig. 3.

Fig. 2 Nondimensional relationship \bar{z} versus \bar{r} Fig. 3 Nondimensional relationship \bar{F} versus \bar{r}

$$\bar{F} = \begin{cases} \bar{r}^2 (\bar{r} + 2\xi) & (1 \leq \bar{r} < \frac{3-\xi}{2}) \\ \frac{3(1+\xi)(3-\xi)^2}{4(1-\xi)} (\bar{r}-1) & (\bar{r} \geq \frac{3-\xi}{2}) \end{cases} \quad (25)$$

As shown in Fig. 3, \bar{F} is nonlinear when $1 \leq \bar{r} < 3-\xi/2$, it then linearly increases as \bar{r} increases when $\bar{r} \geq 3-\xi/2$.

4. Structural efficiency and load-carrying efficiency

In Fig. 2 and Fig. 3, the essential meaning of the turning points can be interpreted based on the

structural efficiency. The structural efficiency is defined as a ratio of the nondimensional critical wrinkling load versus the nondimensional structural weight, and it can be used to reflect the bending capacity per unit structural weight.

Take membrane case as an example, the structural efficiency is defined as

$$\eta = \frac{\bar{F}}{\bar{W}} \times 100\% \quad (26)$$

Where, \bar{F} is the nondimensional critical wrinkling load of membrane case, and it can be given by

$$\bar{F} = \begin{cases} \bar{r}^3 & (1 \leq \bar{r} < 1.5) \\ \frac{27}{4}(\bar{r} - 1) & (\bar{r} \geq 1.5) \end{cases} \quad (27)$$

\bar{W} (in Eq. (26)) is the nondimensional structural weight, which is expressed as

$$\bar{W} = \frac{\rho A_{ic}(\bar{r})t}{\rho \pi r_0^2 t} = \bar{A}(\bar{r}) \quad (28)$$

Here, ρ is the density of the membrane. $A_{ic}(\bar{r})$ is the surface area of the inflated cone. $\bar{A}(\bar{r})$ is the nondimensional structural surface area, which can be expressed as a function of the taper ratio.

$$\bar{A}(\bar{r}) = 1 + \bar{r}^2 + (1 + \bar{r}) \left[z_c^2 + (\bar{r} - 1)^2 \right]^{1/2} \quad (29)$$

Where, $z_c = z_0/r_0$ is the nondimensional structural height.

Based on Eq. (27), Eq. (28) and Eq. (29), we then have the structural efficiency in the form

$$\eta = \frac{\bar{F}}{\bar{A}} \times 100\% = \begin{cases} \frac{\bar{r}^3}{1 + \bar{r}^2 + (1 + \bar{r}) \left[z_c^2 + (\bar{r} - 1)^2 \right]^{1/2}} \times 100\% & (1 \leq \bar{r} < 1.5) \\ \frac{27}{4} \frac{\bar{r} - 1}{1 + \bar{r}^2 + (1 + \bar{r}) \left[z_c^2 + (\bar{r} - 1)^2 \right]^{1/2}} \times 100\% & (\bar{r} \geq 1.5) \end{cases} \quad (30)$$

For a given inflated cone, the taper ratio $\bar{r} = r_1/r_0$ is assumed as a variable parameter, and the other parameters are assumed to be constant. Considered a inflated cone, with 1m height (z_0), 2.5×10^{-2} m free-end radius (r_0), 1×10^4 Pa inflated pressure (P), 3×10^9 Pa Elastic modulus (E) of wall material, 0.34 Poisson ratio (ν), and 2.5×10^{-5} m wall thickness (t), we then obtain the structural efficiency η and plot it in Fig. 4 with increasing taper ratios \bar{r} .

It can be seen from Fig. 4 that the structural efficiency increases as the taper ratio increases. It shows that the structural bending capacity can be improved by increasing taper ratio. However, we still find a turning point occurs at $\bar{r} = 1.5$, after where the curvature has a reversely change. In order to deeply understand the physical essential of this turning point, we perform a further study on the relationship between the structural efficiency and the taper ratio. We defined a concept of the load-carrying efficiency which is the ratio of the incremental structural efficiency versus the incremental taper ratio. The load-carrying efficiency is written as

$$\eta^* = \frac{\Delta\eta}{\Delta\bar{r}} \quad (31)$$

The load-carrying efficiency reflects the influence of the structural geometry on the structural load-carrying ability. It can be regarded as a measure to optimize the geometry of the inflated cone in bending. Fig. 5 depicts a plot of the load-carrying efficiency versus the taper ratio.

Based on Fig. 5, the load-carrying efficiency increases firstly, and then decreases as the taper ratio increases. The load-carrying efficiency reaches the maximum when the taper ratio is equal to 1.5. It reveals that the structural load-carrying ability can not be infinitely improved by increasing the taper ratio, although a higher taper ratio is of benefit to the structural efficiency (Fig. 4). For the bending case, an inflated cone with $\bar{r} = 1.5$ is an optimized geometry which can be designed to behave the highest load-carrying ability.

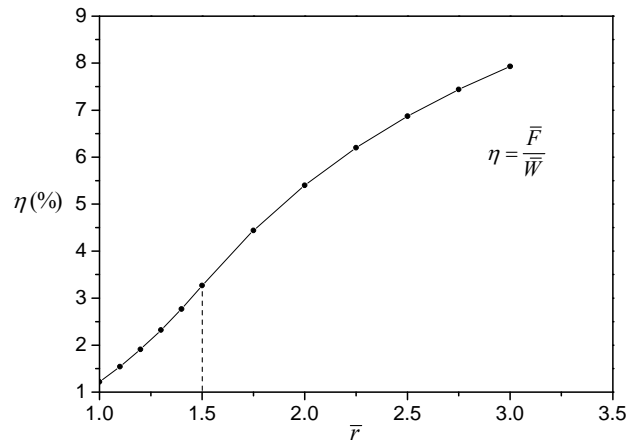


Fig. 4 Relationship η versus \bar{r}

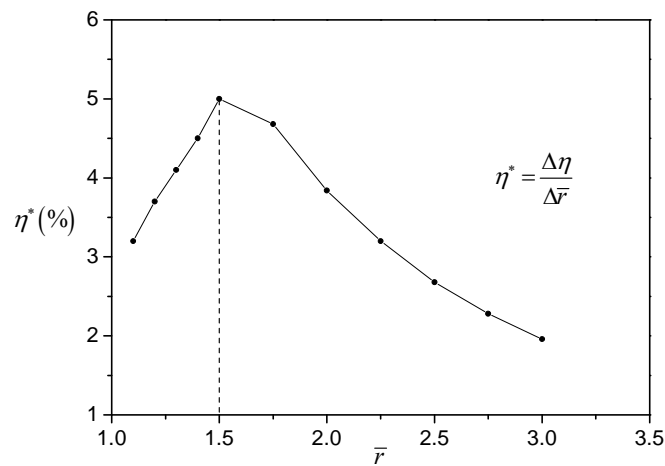


Fig. 5 Relationship η^* versus \bar{r}

5. Numerical verification

A numerical simulation is used to verify the validation of proposed extremum method for the bending-wrinkling predictions of the inflated cone. In this simulation, the structural and material parameters of the inflated cone are the same as those described in SECTION 4. Here the fixed-end radius is given as $r_1=5 \times 10^{-2}m$, which is twice of the free-end radius (i.e., $\bar{r} = 2$). The inflated cone is modeled by using 3200 ANSYS nonlinear SHELL181 elements among which there are 32 hoop elements and 100 axial elements. The Newton-Raphson iteration is used to perform the bending-wrinkling computation.

Here, the minimum principal stress is used to determine the critical wrinkling load and the initial wrinkling location. Here the critical wrinkling load is determined when the minimum principal stress closely reaches the critical compressive stress. The first wrinkle occurs at the location where the minimum principal stress reaches the absolute maximum, as shown in Fig. 6.

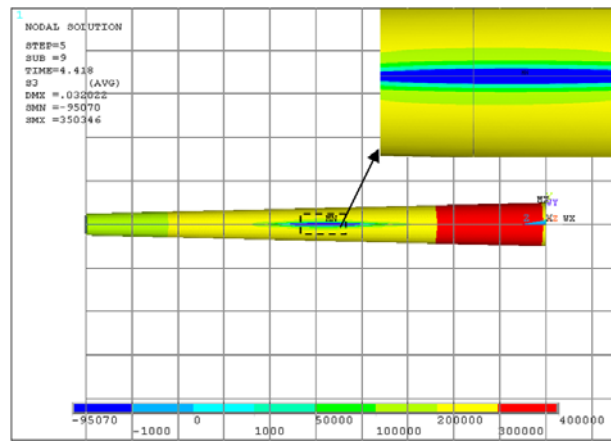


Fig. 6 Initial wrinkling location of inflated cone in bending

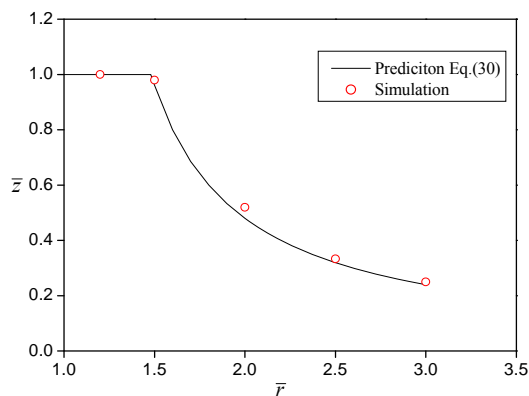


Fig. 7 Comparison of the initial wrinkling location

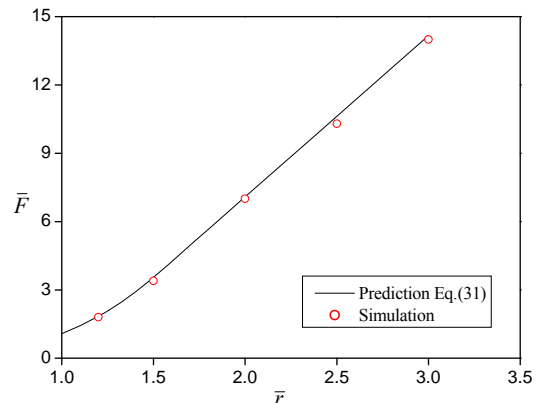


Fig. 8 Comparison of the critical wrinkling load

According to the numerical results, the critical wrinkling load is 1.73N, and the initial wrinkling location is 0.51m far from the free-end of the inflated cone. In our predictions, $r_1 = 2r_0$, and $\xi = 0.04$. Based on Eq. (25), the predictive value of the critical wrinkling load is 1.75N. The initial wrinkling location is 0.48m which is obtained from Eq. (24). These results show that the proposed prediction formula based on beam stress analysis agrees very well with nonlinear shell finite element numerical computations.

In order to obtain the further verifications, five cases of the taper ratio are used to compare the numerical results with our predictions on the critical wrinkling load and the initial wrinkling location. These comparisons are shown in Fig. 7 and Fig. 8, respectively.

Based on Fig. 7, the mean difference in the initial wrinkling location between the simulated and the predicted results is less than 3%. In Fig. 8, the mean difference in the critical wrinkling load is less than 2%. These comparisons show the validation and accuracy of proposed extremum method for the bending-wrinkling predictions of the inflated cone.

6. Conclusions

The extremum method presented in this paper can be accurately used to predict the bending-wrinkling characteristics of the inflated conical cantilever beam. The predictions agree ver well with nonlinear shell finite element numerical computations, which show the validation of extremum method. Based on these results, there important conclusions can be drawn as follows.

- The extremum method is not only suitable for the membrane inflated beam, but can also be used by the thin-shell inflated beam. When the critical compressive stress is considered, the extremum method is extended from the membrane case to the thin-shell case. The initial wrinkling location can be determined by searching the maximum of the wrinkling factor. The initial wrinkling location is changed from the interior to the free-end of the inflated cone with \bar{r} increases. The taper ratio $\bar{r} = 3 - \xi/2$ is a turning point for the initial wrinkling location. In addition, the inflated straight boom is a special case of the inflated cone with case $r_1 = r_0$. For inflated straight booms, the initial wrinkling location occurs at the fixed-end identically.

- The critical wrinkling load is defined as the ratio of the wrinkling moment versus the initial wrinkling location, which can not be directly determined by the ratio of the wrinkling moment versus the total height of the inflated cone. The initial wrinkling location equals to the total height of the inflated cones, if and only if in the case of $1 \leq \bar{r} < 3 - \xi/2$.

- For membrane inflated beam, the critical taper ratio $\bar{r} = 1.5$ corresponds to the highest load-carrying efficiency, which is defined as the ratio of the incremental structural efficiency versus the incremental taper ratio. The load-carrying efficiency increases firstly, and then decreases as the taper ratio increases. It reveals that an inflated cone with the critical taper ratio is an optimized geometry, which can be designed to behave the highest load-carrying ability.

Acknowledgments

The research described in this paper was financially supported by National Natural Science Foundation of China, 11172079; Program for New Century Excellent Talents in University, NCET-11-0807; the Fundamental Research Funds for the Central Universities, HIT.BRETHIII.201209 and HIT.NSRIF.201156.

References

- Comer, R.L. and Levy, S. (1963), "Deflections of an inflated circular-cylindrical cantilever beam", *AIAA J.*, **1**(7), 1652-1655.
- Hampel, J.W., Brown, G.J. and Sharpless, G.S. (1996), "High pressure inflatable structures incorporating highly oriented fibers", *Proc. Twentieth Army Science Conference*.
- Jenkins, C.H. (Ed.) (2001), "Gossamer spacecraft: membrane and inflatable structures technology for space applications", Vol. **191**, *Progress in Astronautics and Aeronautics*, AIAA, Reston, VA, 1-46.
- Jenkins, C.H. (Ed.) (2006), "Recent advances in gossamer spacecraft: Chapter 3 Membrane wrinkling", Vol. **212**, *Progress in Astronautics and Aeronautics*, AIAA, Reston, VA, 109-164.
- Main, J.A., Peterson, S.W. and Strauss, A.M. (1994), "Load-deflection behavior of space-based inflatable fabric beams", *J. Aerosp. Eng.*, **2**(7), 225-238.
- Norris, R.K. and Pulliam, W.J. (2009), "Historical perspective on inflatable wing structures", *50th AIAA/ASME/ASCE/AHS/ASC Structures, Structural Dynamics, and Materials Conference*, May, Palm Springs, California, AIAA 2009-2145.
- Quigley, C.J., Cavallaro, P.V., Johnson, A.R. and Sadegh, A.M. (2003), "Advances in fabric and structural analyses of pressure inflated structures", *Proc. IMECE'03 2003 ASME Int. Mechanical Engineering Congress*, ASME International, New York, 19-25.
- Stein, M. and Hedgepeth, J.M. (1961), "Analysis of partly wrinkled membranes", NASA, *Tech Note*, D-813.
- Thomas, J.C. and Wielgosz, C. (2004), "Deflections of highly inflated fabric tube", *Thin Wall Struct.*, **42**(7), 1049-1066.
- Veldman, S.L. (2003), "Load analysis of inflatable truncated cones", *44th AIAA/ASME/ASCE/AHS/ASC Structures, Structural Dynamics, and Materials Conference*, April, Norfolk, Virginia, AIAA 2003-1827.
- Veldman, S.L., Bergsma, O.K. and Beukers, A. (2005), "Bending of anisotropic inflated cylindrical beams", *Thin Wall Struct.*, **43**(3), 461-475.
- Veldman, S.L., Beukers, A. and Bergsma, O.K. (2006a), "Wrinkling prediction of cylindrical and conical inflated cantilever beams under torsion and bending", *Thin Wall Struct.*, **44**(2), 211-215.
- Veldman, S.L. and Bergsma, O.K. (2006b), "Analysis of inflated conical cantilever beams in bending", *AIAA J.*, **44**(6), 1345-1349.
- Wang, C.G., Tan, H.F., Wan, Z.M. and BAIER, H. (2009a), "A new model for bending-wrinkling analysis of membrane inflated beam", *International Conference on Textile Composites and Inflatable Structures*, Structural Membranes, Stuttgart, October.
- Wang, C.G., Du, X.W. and Wan, Z.M. (2006), "Numerical simulation of wrinkles in space inflatable structures", *J. Spacecr. Rockets*, **43**(5), 1146-1149.
- Wang, C.G., Tan, H.F., Du, X.W. and Wan, Z.M. (2007), "Wrinkling prediction of rectangular shell-membrane under transverse in-plane displacement", *Int. J. Solids Struct.*, **44**(20), 6507-6516.
- Wang, C.G., Du, X.W., Tan, H.F. and He, X.D. (2009b), "A new computational method for wrinkling analysis of gossamer space structures", *Int. J. Solids Struct.*, **46**(6), 1516-1526.
- Wang, C.G., Du, X.W. and He, X.D. (2008), "Wrinkling analysis of space inflatable membrane structures", *Chin. J. Theor. Appl. Mech.*, **40**(3), 331-337.
- Wang, C.G., Du, X.W. and He, X.D. (2009c), "Bending-wrinkling behavior analysis for inflatable membrane boom", *Eng. Mech.*, **26**(2), 210-215.
- Wood, J.D. (1958), "The flexure of a uniformly pressurized, circular, cylindrical shell", *J. Appl. Mech.*, **25**(12), 453-461.
- Wielgosz, C. and Thomas, J.C. (2002), "Deflections of inflatable fabric panels at high pressure", *Thin Wall Struct.*, **40**(6), 523-536.
- Zender, G.W. (1962), "The bending strength of pressurized cylinders", *J. Aerosp. Sci.*, **29**(3), 362-365.